Hindawi
Shock and Vibration
Volume 2019, Article ID 9135412, 19 pages
https://doi.org/10.1155/2019/9135412

Research Article

Simulation of the Vibration Characteristics for Agricultural Wheeled Tractor with Implement and Front Axle Hydropneumatic Suspension

Enlai Zheng, Song Cui, Yuanzhao Yang, Jinlin Xue, Yue Zhu, and Xiangze Lin

Department of Mechanical Engineering, College of Engineering, Nanjing Agricultural University, Nanjing 210031, China

Correspondence should be addressed to Enlai Zheng; enlaizheng@njau.edu.cn

Received 9 April 2019; Revised 13 June 2019; Accepted 23 June 2019; Published 7 July 2019

Academic Editor: Edoardo Sabbioni

The dynamic model is significant for the analysis of the vibrational characteristics of the wheeled tractor system with implement and front axle hydropneumatic suspension. In this work, the nonlinear stiffness and damping equations are derived first. The dynamic coupling relationship among cabin, three-point hitch structure, and implement are figured out, and the dynamic model of the half agricultural wheeled tractor/implement system is presented considering the effects of three-point hitch structure, passive silent blocks of cabin, and front axle hydropneumatic suspension together. To validate the model, the power spectral densities (PSDs) of the driver seat, cabin, chassis, and implement acquired from numerical simulations are compared with those from experiments, respectively. Under different forward speeds, two groups of results match well. Based on the model, the influences of passive cabin suspension, implement, and front axle hydropneumatic suspension on the dynamical characteristics of the tractor system are investigated. Results indicate that the front axle hydropneumatic suspension will deteriorate the ride comfort of the driver but improve the handing stability. The passive cabin suspension reduces the operational stability while improving much more ride comfort than the front axle hydropneumatic suspension does. The driver's comfortableness will be increased due to implement; meanwhile, handling stability will be compromised. Besides, the impacts of initial nitrogen volume, pressure of accumulators, and orifice diameter of throttle valves on the vibration characteristics of the tractor system are also inspected.

1. Introduction

The low-frequency vibration experienced by an agricultural tractor comes from the interaction between the tractor and the rough terrain [1–4]. It is severe when primary tractors only have the tires as the elastic component between the road and the tractor [5, 6], for the reason that tires are unable to provide proper suspension characteristics required to absorb these vibrations. According to the International Standard (ISO) 2631-1:1997 [7], daily exposure to whole body vibration (WBV) among tractor drivers may lead to adverse effects on health such as musculoskeletal disorder and low back pain [8]. The primary contact point for transmission of vertical WBV to drivers is through the tractor seat (amplifies or attenuates vibration at the base). It should be noted that the human-sensitive frequency range for vertical vibration is from 4 to 8 Hz. Seat effective amplitude transmissibility (SEAT) value is also used to represent the efficiency of seat isolation.

Moreover, the tractor vibration leads to the tires' dynamic load on the ground, which will not only damage the road and intensify farmland soil compaction [9–13] but also affect the handling stability of the tractor. With the development of technology, the front axle of a modern tractor has been equipped with the hydropneumatic suspension. Therefore, it is essential to develop a dynamic model of the tractor/implement system with front axle suspension to predict its vibration characteristics and evaluate its

performances, which provides a theoretical basis for structural design and parameter optimization of both the suspension and tractor system.

The main feature of this work is that it considers the hydropneumatic suspension on the front axle, the three-point hitch structure between implement and tractor frame, and excitations from ground surface roughness, which leads to strong nonlinear dynamics. There are six degrees of freedom (DOF) related to the tractor body motions including three-dimensional and three rotational degrees of freedom. Thus, it is challenging to establish an integrated dynamic model of the wheeled tractor/implement system with the hydropneumatic suspension on the front axle.

In order to investigate the vibration characteristics of agricultural wheeled tractors, there have been two main approaches. One is the experimental approach, and the other is the computer simulation method. In the aspect of the experimental approach, Clijmans et al. [14] used the experimental modal analysis technique to predict the structural behaviour of the machine under a set of excitation conditions. When studying the effects of vibration on drivers, Cutini et al. [15] operated three agricultural tractors on six test tracks at different forward speeds to evaluate the whole body vibration of the agricultural tractor's operator. Adam and Jalil [16] performed measurements on a healthy male tractor driver to determine the vertical suspension seat transmissibility and SEAT values. In addition, some researchers measured the vertical vibration accelerations of the front axles, rear axles, and cabin for the two-wheel-drive tractor under different road conditions and forward speeds [17–19]. Also, Nguyen and Inaba [20] measured the vertical wheel load of the left and right rear wheels and the roll, bounce, and pitch accelerations of the rear axle center on an asphalt road and a sandy loam field. Although the experimental method can provide more precise and reliable results, high expenses, insecurity, and inconvenience limit its development. Moreover, Yang et al. [21] pointed out that the results from an experiment are based on the specified test tractor and field conditions, which did not suit other test conditions.

Compared with the experimental approach, the computer simulation method employs the mathematical models or multibody dynamic models constructed by commercial software to extrapolate the experimental results over the range of test conditions [22, 23]. The quarter-vehicle model, half-vehicle model, and full-vehicle body models have been developed to predict the dynamic behaviour of the tractor and to carry out the vibration control. Especially the one-dimensional quarter-vehicle models with single or two DOF are commonly used to study the heave motion of the tractor body [24]. Cuong et al. [4] modeled tire-soil system as an equivalent system by the mechanism of a linear parallel spring and damper in vertical the direction with one end connected to the tire axle and the other end connected to the hard layer. To calculate the structural parameters of the hydropneumatic spring, Yuan et al. [25] established a vibration model of the front axle suspension tractor and the stiffness and damping nonlinear mathematical model of the hydropneumatic spring.

The two-dimensional half-vehicle model represents the tractor's longitudinal dynamics using the heave and pitch motion of the tractor body and the vertical motion of the front and rear wheels [26–28]. In order to study the influence of implement's mass on the vibration characteristics of the tractor/implement system, Zhu et al. [29] established a two-degree-of-freedom vibration model of the tractor with a rear implement. On this basis, Zheng et al. [30] developed a complete nonlinear dynamic model of the wheeled tractor with a suspended driver seat including air spring and MR damper, and the effects of nonlinear stiffness for scissors linkage seat, the air spring with auxiliary chamber as well as MR damper, and dynamic characteristics of real tire are also considered in this model. The presented half-vehicle model can also be used to describe the lateral dynamics, with the roll and heave motion of the tractor body and the vertical motion of the left and right wheels.

The three-dimensional full-tractor model has various number of DOFs, which starts from six DOFs up to hundreds. The concrete number depends on the number of components being modeled, the model versatility, and the simplifying assumptions being used [31]. For example, in a multibody model of a tractor, Melzi et al. [32] used not only the spring-damper elements to represent the suspension system but also the rigid body to represent vehicle chassis, cabin, and the seat with different DOFs (yaw, pitch, and roll). Considering that the tractor consists of a rotatable front end (anterior part) and the main body (posterior part), Li et al. [33] analysed the pitch motion of the front part of the tractor as well as the roll motion of the rear part of the tractor and predicted tractor behaviour when a tire is off the ground. In vehicle driving simulations, Sim et al. [34] established three-dimensional vehicle dynamic models containing the seat, cabin, body, and tires with a 14-DOF model which describes the bounce, pitch, roll, longitudinal response, and lateral response of the tractor's seat, cabin, and tire.

In addition to the cabin and driver seat suspension [35–37], to improve the driver's comfort and the steering response, front axle suspension is always the focus of this research. For the tractor without implement, Martelli et al. [38] pointed out the front axle elastic suspension had limited effect on the vertical vibration and driving safety depending on the driving conditions, while its effect on the pitch and lateral vibration is obvious [28]. Furthermore, Mazhei et al. [39] found that when the implement is mounted in front of a tractor, the effect of the front axle elastic suspension relies on the damping element, but it was less effective than that without front implement. Apart from the linear elastic front axle suspension, the researchers also designed the hydropneumatic nonlinear suspension as the front axle suspension of the tractor.

When studying the output force of hydropneumatic suspension, Theron and Els [40] considered mathematical modelling of a suspension unit that comprises a hydraulic cylinder connecting the vehicle body to the unsprung mass, two nitrogen-filled accumulator springs, and two damper ports. van der Westhuizen and Schalk Els [41] developed an

accurate suspension model to obtain realistic vehicle dynamics simulation results when considering different suspension characteristics or control algorithms. Considering polytropic change in the gas state and seal friction, the gas-oil emulsion flows through orifices and valves. Yin et al. [42] formulated an analytical model of the hydropneumatic suspension, which considers one and two bleed orifices configurations of the strut. Eventually, the validity of these mathematical models is proved by the experimental rig in the lab. Unlike the conventional linear elastic front axle suspension, Yilidaer et al. [43] found that the hydropneumatic nonlinear suspension plays an important role in reducing the vertical vibration acceleration and pitching vibration angular acceleration of the tractor.

As far as we know, few attempts have been made to study the effect of the front axle hydropneumatic suspension along with the passive cabin suspension on the vibration characteristics of the agricultural tractor/implement system including the structure of three-point hitch. In this work, the dynamic model of the wheeled tractor/implement system with hydropneumatic suspension on the front axle is established and the vibration characteristics in both time and frequency domains are analysed. Furthermore, the effect of forward speed, nitrogen volume, and pressure of accumulators and orifice area of proportional and throttle valves on the vibration characteristics of the tractor system are also investigated.

2. Tractor/Implement Description

As shown in Figure 1, the rodless chamber 1 in the front axle hydropneumatic suspension system is connected with the accumulator A using the proportional valve 5 and the small throttle valve 6. While the rod chamber in the cylinder 1 is connected in series with the accumulator B via the proportional valve 7 and the small throttle valve 8. The large throttle valve 10 is installed between the accumulators A and C to adjust the oil pressure between the rod and rodless chambers of cylinder 1, and the membrane-coated cylinders of the accumulators A, B, and C can isolate the nitrogen through valve block 3 and ball valve 4.

The piston rod 2 is hinged to the front axle, and the cylinder 1 of the hydropneumatic suspension is hinged to the chassis. Running on rough ground, the tractor's piston rod reciprocates in the cylinder due to the relative motion between the front axle and the chassis. Once the front axle comes close to the chassis and the throttle valve 9 is closed, the hydropneumatic suspension is compressed and the volume of the rodless chamber will be reduced. As a consequence of the oil pressure increase in the rodless chamber 1, the oil flows to the accumulator A through the proportional valve 5 and the small throttle valve 6. Meanwhile, the oil pressure of the rod chamber is lessened, making the oil in the accumulator B flow to the pole room. The proportional valve 7 and the small throttle valve 8 are used to adjust the oil pressure. The flow direction of oil will be opposite to the above direction if the front axle is separated from the chassis. When the throttle valve 9 is opened, part of oil in the rodless and rod chambers will form a closed oil circuit.

As can be seen in Figure 2(a), the wheeled tractor with implements consists of the chassis, front and rear axles, tires, cabin, driver seat, and implement. The implement is connected to the tractor body via the three-point hitch structure shown in Figure 2(b). The three-point suspension is composed of a lifting shaft, a lifting arm, an upper connecting rod, a lifting link, a lower connecting rod, and a plow mounting bracket. Once the lift shaft starts to rotate, the lift link and the upper link will get the plow mounting bracket off the ground. Between the cabin and the chassis, passive silent blocks are set up to improve the ride comfort, as shown in Figure 2(c).

3. Dynamic Model of Tractor/Implement System with Front Axle Hydropneumatic Suspension

The upper and lower ends of the cylinder for the hydropneumatic suspension are hinged to the front axle and the chassis, respectively. The tractor body structure is represented by mass and moment of inertia relative to a central axis perpendicular to the symmetry plane. A dynamic model of the wheeled tractor with the implement and front axle hydropneumatic suspension system was developed, as shown in Figure 3. The front and rear tires of the tractor system are subjected to the displacement excitations $q_{fz}(t)$ and $q_{rz}(t)$, respectively, since there is a difference between the amplitudes $q_{fz}(t)$ and $q_{rz}(t)$ and the angular displacement with respect to the mass center arises.

The ground excitation relation between the front and rear axles of the tractor/implement system at the instant i by considering the time lag τ between $q_{fzi}(t)$ and $q_{rzi}(t)$ can be expressed by

$$q_{fzi}(t) = q_{rzi}(t+\tau), \tag{1}$$

where $q_{fzi}(t)$ and $q_{rzi}(t)$ are the displacement excitations at front and rear axles, respectively, τ is the time lag and can be calculated as $(l_{bf}+l_{br})/v$, l_{bf} is the distance of the mass center between the chassis and the front axle, l_{br} is the distance of the mass center between the chassis and the rear axle, and v is the velocity of the tractor/implement system.

The governing equations of motion for the front axle suspension and cabin as well as driver seat can be given by

$$m_e\ddot{z}_e = F_p - k_f(z_e - q_f) - c_f(\dot{z}_e - \dot{q}_f), \tag{2a}$$

$$\begin{aligned} m_c\ddot{z}_c = {} & k_{cr}(z_b + l_{br}\varphi_b - z_c - l_{cr}\varphi_c) \\ & + c_{cr}(\dot{z}_b + l_{br}\dot{\varphi}_b - \dot{z}_c - l_{cr}\dot{\varphi}_c) \\ & + k_{cf}(z_b - z_c + l_{cf}\varphi_c - l_{bf}\varphi_b) \\ & + c_{cf}(\dot{z}_b - \dot{z}_c + l_{cf}\dot{\varphi}_c - l_{bf}\dot{\varphi}_b) - k_d(z_c + l_d\varphi_c - z_d) \\ & - c_d(\dot{z}_c + l_d\dot{\varphi}_c - \dot{z}_d), \end{aligned} \tag{2b}$$

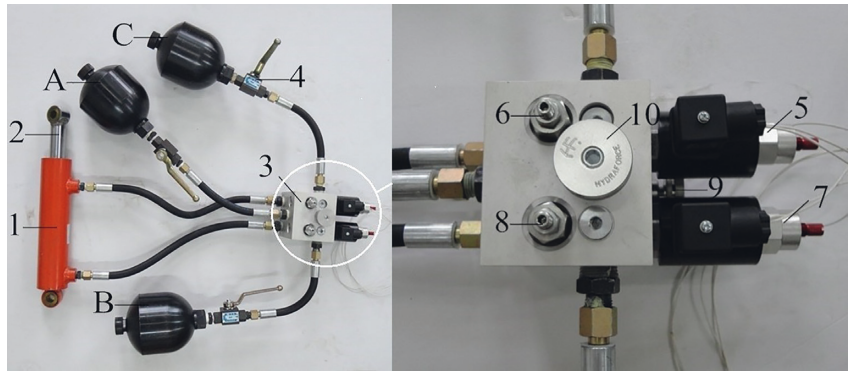

Figure 1: Physical structure of the front axle hydropneumatic suspension system.

(a) (b) (c)

Figure 2: Physical structure of the tractor system: (a) tractor/implement system; (b) three-point hitch structure; (c) silent blocks of cabin.

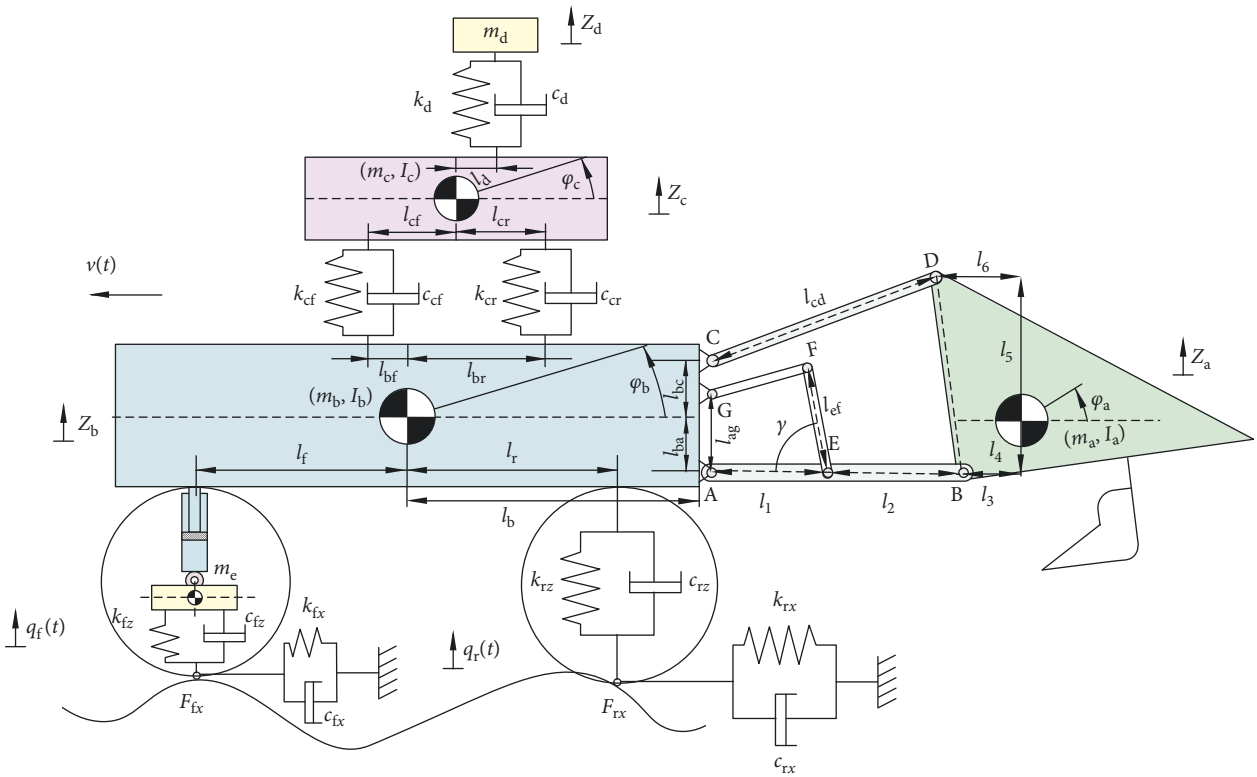

Figure 3: Dynamic model of the wheeled tractor system with the implement and front axle hydropneumatic suspension.

$$I_c\ddot{\varphi}_c = [k_{cr}(z_b + l_{br}\varphi_b - z_c - l_{cr}\varphi_c) + c_{cr}(\dot{z}_b + l_{br}\dot{\varphi}_b - \dot{z}_c - l_{cr}\dot{\varphi}_c)]l_{cr} - [k_{cf}(z_b - z_c + l_{cf}\varphi_c - l_{bf}\varphi_b) + c_{cf}(\dot{z}_b - \dot{z}_c + l_{cf}\dot{\varphi}_c - l_{bf}\dot{\varphi}_b)]l_{cf} - [k_d(z_c + l_d\varphi_c - z_d) + c_d(\dot{z}_c + l_d\dot{\varphi}_c - \dot{z}_d)]l_d, \quad (2c)$$

$$m_d\ddot{z}_d = k_d(z_c + l_d\varphi_c - z_d) + c_d(\dot{z}_c + l_d\dot{\varphi}_c - \dot{z}_d). \quad (2d)$$

3.1. Model of Front Axle Hydropneumatic Suspension. The large throttle valve 10 is usually closed and can be used to control the volume of the accumulator A. The influences of the accumulator C can be neglected. The model of the front axle hydrosuspension is developed, as shown in Figure 4. Compared with the nitrogen, the oil in the accumulator can be perceived as an incompressible flow. Therefore, the force produced by the piston rod can be given by

$$F_h = P_1A_1 - P_2A_2, \quad (3)$$

where P_1 and P_2 are the transient pressures of the rod cavity and of the rodless cavity, respectively, A_1 is the area of the piston with $A_1 = \pi D^2/4$, D denotes the diameter of the piston, A_2 represents the effective area of the rod cavity with $A_2 = \pi(D^2 - d^2)/4$, and d stands for the diameter of the piston rod.

The orifice size of the front axle hydropneumatic suspension is very small, so is that of the proportional valve. Based on this, the oil flow can be calculated as

$$q = C_dA\sqrt{\frac{2\Delta P}{\rho}}, \quad (4)$$

where ρ is the density of oil, A is the flow area of the hole that mounts the throttle and proportional valves, C_d denotes the flow coefficient of the hole, and ΔP represents the pressure difference between the oil cavity and the accumulator.

The compression on the hydropneumatic suspension will cause the oil in the rodless chamber 1 to flow into the accumulator A via the throttle valve 6 and the proportional valve 5; meanwhile, the oil in the accumulator B passes through the throttle valve 8 and the proportional valve 7 and enters the rod cavity 2. When the hydropneumatic suspension rebounds, the flow direction of the oil will be reversed. The numerical relationship between the flow rate and the speed of the piston rod can be described by

$$A_1\dot{x} = \mathrm{sgn}(\dot{x})\left[C_dA_9\sqrt{\frac{2\Delta P_{21}}{\rho}} + C_d(A_5 + A_6)\sqrt{\frac{2\Delta P_{A1}}{\rho}}\right], \quad (5a)$$

$$A_2\dot{x} = \mathrm{sgn}(\dot{x})\left[C_dA_9\sqrt{\frac{2\Delta P_{21}}{\rho}} + C_d(A_7 + A_8)\sqrt{\frac{2\Delta P_{2B}}{\rho}}\right], \quad (5b)$$

where A_6 and A_8 denote the flow area of the throttle valves 6 and 8, respectively, A_5 and A_7 are the flow area of the proportional valves 5 and 7, A_9 is the flow area of the throttle valve 9, ΔP_{1A} is the absolute value of the oil pressure difference between the rodless cavity 1 and the accumulator A, ΔP_{2B} is the absolute value of the oil pressure difference between the rod cavity 2 and the accumulator B, $\mathrm{sgn}(\dot{x})$ is the symbolic function, and $\dot{x}$ is the relative velocity between the chassis and front axle with $\dot{x} = \dot{z}_b - l_f\dot{\varphi}_b - \dot{z}_e$.

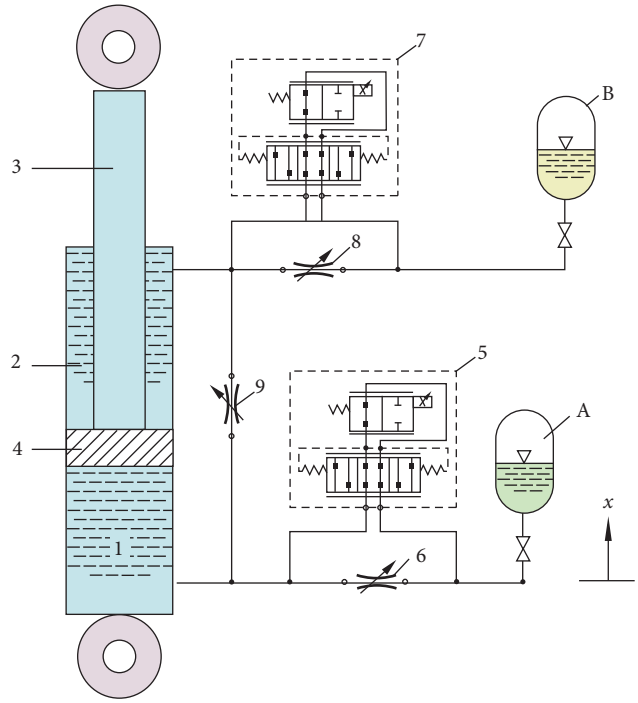

Figure 4: Model of front axle hydropneumatic suspension.

The symbolic function is

$$\mathrm{sgn}(\dot{x}) = \begin{cases} 1, & \dot{x} > 0, \\ 0, & \dot{x} = 0, \\ -1, & \dot{x} < 0. \end{cases} \quad (6)$$

The velocity with respect to the volume change of the accumulators A and B can be expressed as

$$\begin{cases} \mathrm{sgn}(\dot{x})C_d(A_5 + A_6)\sqrt{\frac{2\Delta P_{A1}}{\rho}}dt = \dot{V}_A, \\ \mathrm{sgn}(\dot{x})C_d(A_7 + A_8)\sqrt{\frac{2\Delta P_{2B}}{\rho}}dt = -\dot{V}_B. \end{cases} \quad (7)$$

It is assumed that the gas in accumulators is ideal and its temperature is considered to be invariant. Thus, the state equation of this ideal gas will be

$$P_AV_A = P_{A0}V_{A0}, \quad P_BV_B = P_{B0}V_{B0}, \quad (8)$$

where P_A represents the transient pressure of the accumulator A; V_A is the transient volume of the accumulator A;

likewise, P_B and V_B denote the transient pressure and the transient of the accumulator B; P_{A0} and V_{A0} are the initial pressure and the initial volume of the accumulator A, and P_{B0} and V_{B0} are the initial pressure and the initial volume of the accumulator B.

According to the state equation of the ideal gas, the oil pressure of the accumulators A and B can be expressed as

$$P_A = \frac{P_{A0}V_{A0}}{V_{A0} - A_1 x},$$
$$P_B = \frac{P_{B0}V_{B0}}{V_{B0} + A_2 x}, \tag{9}$$

where x is the relative displacement between the chassis and the front axle, $x = z_b - l_f\varphi_b - z_e$.

Based on equation (8), the derivatives of the volume change of the accumulators A and B with respect to time are

$$\dot{V}_A = \frac{-P_{A0}V_{A0}\dot{P}_A}{P_A^2},$$
$$\dot{V}_B = \frac{-P_{B0}V_{B0}\dot{P}_B}{P_B^2}. \tag{10}$$

By solving equation (5), the oil pressure can be given by

$$P_1 = P_A - \frac{\left[\rho P_{A0}^2 V_{A0}^2 \left(\dot{P}_A/P_A\right)^2 \mathrm{sgn}(\dot{x})\right]}{\left[2C_d^2\left(A_5 + A_6\right)^2\right]},$$
$$P_2 = P_B + \frac{\left[\rho P_{B0}^2 V_{B0}^2 \left(\dot{P}_B/P_B\right)^2 \mathrm{sgn}(\dot{x})\right]}{\left[2C_d^2\left(A_7 + A_8\right)^2\right]}. \tag{11}$$

Friction force between the cylinder and the piston can be

$$F_f(\dot{x}) = \mathrm{sgn}(\dot{x})\left[F_c + (F_s - F_c)e^{-\left(\dot{x}/\dot{x}_s\right)^2} + f_v\dot{x}\right], \tag{12}$$

where F_c is the Coulomb friction force, F_s is static friction force, f_v is the coefficient of the viscous friction force, and $\dot{x}_s$ is the Stribeck velocity.

The total force acting on the piston rod with the damping force of the orifice and the friction force between cylinder and piston considered can be given by

$$F_p = F_h - F_f. \tag{13}$$

The throttle valve 9 will be either closed or fully opened. When the throttle valve 9 is in the closed state, the force of the hydropneumatic suspension can be calculated as

$$F_p = \frac{\rho A_1^3 \dot{x}^2 \mathrm{sign}(\dot{x})}{2C_d^2\left(A_j + A_c\right)^2} + \frac{P_{A0}V_{A0}^r A_1}{\left(V_{A0} - A_1 x\right)^r} - \mathrm{sign}(\dot{x})\left[F_c + (F_s - F_c)e^{-\left(\dot{x}/\dot{x}_s\right)^2} + F_v\dot{x}\right] - \frac{P_{B0}V_{B0}^r A_2}{\left(V_{B0} + A_2 x\right)^r} + \frac{\rho A_2^3 \dot{x}^2 \mathrm{sign}(\dot{x})}{2C_d^2\left(A_z + A_d\right)^2}. \tag{14}$$

Otherwise, the force of the hydropneumatic suspension can be expressed as

$$F_p = \frac{P_{A0}\left(V_{A0} + V_{B0}\right)\left(A_1 - A_2\right)}{\left[P_{A0}\left(V_{A0} + V_{B0}\right)\left(A_1 - A_2\right)/(\mathrm{Mg}) - \left(A_1 - A_2\right)x\right]} + \left[\frac{\rho\left(A_1 - A_2\right)^3\dot{x}^2}{4C_d^2\left(A_5 + A_6\right)^2} + \frac{\rho\left(A_1 - A_2\right)^3\dot{x}^2}{4C_d^2\left(A_7 + A_8\right)^2} - F_c - \left(F_s - F_c\right)e^{-\left(\dot{x}/\dot{x}_s\right)^2} - F_v\dot{x}\right]\mathrm{sign}(\dot{x}). \tag{15}$$

3.2. Model of Three-point Hitch Structure. The model of the three-point hitch structure is shown in Figure 5. Separating the upper link CD from the three-point hitch structure, its force balance relationship can be given by

$$\begin{aligned} &F_{dx} - F_{cx} - m_2 a_{2x} = 0,\\ &F_{cz} - F_{dz} - m_2 g - m_2 a_{2z} = 0,\\ &F_{dx}\left(l_{cd} - l_{cm}\right)\sin\varphi_2 + F_{dz}\left(l_{cd} - l_{cm}\right)\cos\varphi_2\\ &\quad + F_{cx}l_{cm}\sin\varphi_2 + F_{cz}l_{cm}\cos\varphi_2 = I_2\ddot{\varphi}_2. \end{aligned} \tag{16}$$

Similarly, the force balance relation of the implement can be expressed as

$$\begin{aligned} F_{bx} - F_{dx} &= 0,\\ F_{dz} - m_a g - m_a\ddot{z}_a - F_{bz} &= 0,\\ F_{bx}l_4 + F_{bz}l_3 + F_{dx}l_5 - F_{dz}l_6 &= I_a\ddot{\varphi}_a. \end{aligned} \tag{17}$$

Separating the lower link AB from the three-point hitch structure, its force balance relation can be expressed as

$$\begin{aligned} &F_{ax} - F_{bx} - m_1 a_{1x} + F_e\cos\left(\gamma - \varphi_1\right) = 0,\\ &F_{bz} - F_e\sin\left(\gamma - \varphi_1\right) - F_{az} - m_1 g - m_1 a_{1z} = 0,\\ &-F_{bz}\left(l_1 + l_2 - l_{am}\right)\cos\varphi_1 - F_{az}l_{am}\cos\varphi_1 - F_e\sin\gamma\left(l_{am} - l_1\right)\\ &\quad - F_{bx}\left(l_1 + l_2 - l_{am}\right)\sin\varphi_1 - F_{ax}l_{am}\sin\varphi_1 = I_1\ddot{\varphi}_1. \end{aligned} \tag{18}$$

Similarly, the force balance relation of the chassis can be given by

$$m_b\ddot{x}_b = F_{ax} - F_{cx} + F_e\cos\left(\gamma - \varphi_1\right) + F_{fx} + F_{rx}, \tag{19a}$$

$$\begin{aligned} m_b\ddot{z}_b = &-F_p + k_r\left(q_r - z_b - l_r\varphi_b\right) + c_r\left(\dot{q}_r - \dot{z}_b - l_r\dot{\varphi}_b\right)\\ &- k_{cr}\left(z_b - z_c - l_{cr}\varphi_c + l_{br}\varphi_b\right)\\ &- c_{cr}\left(\dot{z}_b - \dot{z}_c - l_{cr}\dot{\varphi}_c + l_{br}\dot{\varphi}_b\right)\\ &- k_{cf}\left(z_b - z_c + l_{cf}\varphi_c - l_{bf}\varphi_b\right)\\ &- c_{cf}\left(\dot{z}_b - \dot{z}_c + l_{cf}\dot{\varphi}_c - l_{bf}\dot{\varphi}_b\right)\\ &+ F_{cz} - F_e\sin\left(\gamma - \varphi_1\right) - F_{az}, \end{aligned} \tag{19b}$$

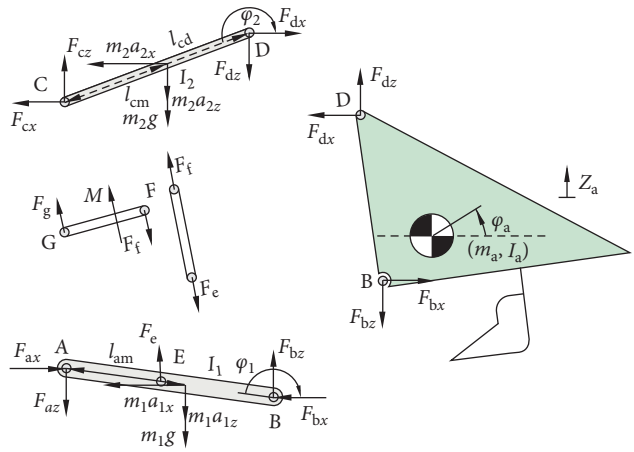

Figure 5: Model of three-point hitch structure.

$$\begin{aligned} I_b\ddot{\varphi}_b = {} & F_p l_f + [k_r(q_r - z_b - l_r\varphi_b) + c_r(\dot{q}_r - \dot{z}_b - l_r\dot{\varphi}_b)]l_r \\ & - [k_{cr}(z_b - z_c - l_{cr}\varphi_c + l_{br}\varphi_b) \\ & + c_{cr}(\dot{z}_b - \dot{z}_c - l_{cr}\dot{\varphi}_c + l_{br}\dot{\varphi}_b)]l_{br} \\ & + [k_{cf}(z_b - z_c + l_{cf}\varphi_c - l_{bf}\varphi_b) \\ & + c_{cf}(\dot{z}_b - \dot{z}_c + l_{cf}\dot{\varphi}_c - l_{bf}\dot{\varphi}_b)]l_{bf} + F_{cx}l_{bc} \\ & + F_{cz}l_b - F_e\cos(\gamma - \varphi_1)(l_{ag} - l_{ba}) \\ & - F_e\sin(\gamma - \varphi_1)l_b + F_{ax}l_{ba} - F_{az}l_b \\ & - F_{fx}(z_b - q_f) - F_{rx}(z_b - q_r). \end{aligned} \tag{19c}$$

The force balance relation of the implement can be expressed as

$$\begin{aligned} F_{bx} &= F_{dx}, \\ F_{dz} - F_{bz} - m_a g &= m_a\ddot{z}_a, \\ F_{bx}l_4 + F_{bz}l_3 + F_{dx}l_5 - F_{dz}l_6 &= I_a\ddot{\varphi}_a. \end{aligned} \tag{20}$$

The angular velocity and acceleration of link CD can be described as

$$\begin{cases} \ddot{\varphi}_2 = \dfrac{a_{dx}\sin\varphi_2 - a_{dz}\cos\varphi_2 - a_{cx}\sin\varphi_2 + a_{cz}\cos\varphi_2}{l_{cd}}, \\ \dot{\varphi}_2 = \left[\dfrac{a_{dz}\sin\varphi_2 - a_{dx}\cos\varphi_2 - a_{cz}\sin\varphi_2 + a_{cx}\cos\varphi_2}{l_{cd}}\right]^{1/2}, \end{cases} \tag{21}$$

where $a_{dz} = \ddot{z}_a - l_6\ddot{\varphi}_a - l_5\dot{\varphi}_a^2$, $a_{dx} = -l_5\ddot{\varphi}_a + l_6\dot{\varphi}_a^2$, $a_{cz} = \ddot{z}_b + l_b\ddot{\varphi}_b - l_{bc}\dot{\varphi}_b^2$, and $a_{cx} = -l_{bc}\ddot{\varphi}_b - l_b\dot{\varphi}_b^2$.

The acceleration at the mass center of link CD in the horizontal and vertical directions can be expressed as

$$\begin{cases} a_{2x} = a_{cx} + l_{cm}\ddot{\varphi}_2\sin\varphi_2 + l_{cm}\dot{\varphi}_2^2\cos\varphi_2, \\ a_{2z} = a_{cz} - l_{cm}\ddot{\varphi}_2\cos\varphi_2 + l_{cm}\dot{\varphi}_2^2\sin\varphi_2. \end{cases} \tag{22}$$

Similarly, the angular velocity and acceleration of link AB can also be given by

$$\begin{cases} \ddot{\varphi}_1 = \dfrac{(-\ddot{z}_a\cos\varphi_1 + l_3\cos\varphi_1\ddot{\varphi}_a + l_4\sin\varphi_1\ddot{\varphi}_a - l_4\cos\varphi_1\dot{\varphi}_a^2 + l_3\sin\varphi_1\dot{\varphi}_a^2 + \ddot{z}_b\cos\varphi_1 + l_b\cos\varphi_1\ddot{\varphi}_b - l_{ba}\sin\varphi_1\ddot{\varphi}_b + l_{ba}\cos\varphi_1\dot{\varphi}_b^2 + L_b\sin\varphi_1\dot{\varphi}_b^2)}{l_{ab}}, \\ \dot{\varphi}_1 = \left[\dfrac{(-\ddot{z}_b\sin\varphi_1 - l_b\sin\varphi_1\ddot{\varphi}_b - l_{ba}\cos\varphi_1\ddot{\varphi}_b - l_{ba}\sin\varphi_1\dot{\varphi}_b^2 + l_b\cos\varphi_2\dot{\varphi}_b^2 + \ddot{z}_a\sin\varphi_1 - l_3\sin\varphi_1\ddot{\varphi}_a + l_4\cos\varphi_1\ddot{\varphi}_a + l_4\sin\varphi_1\ddot{\varphi}_a + l_3\cos\varphi_1\dot{\varphi}_a^2)}{l_{ab}}\right]^{1/2}, \end{cases} \tag{23}$$

where $a_{bx} = l_4\ddot{\varphi}_a + l_3\dot{\varphi}_a^2$, $a_{bz} = \ddot{z}_a - l_3\ddot{\varphi}_a + l_4\dot{\varphi}_a^2$, $a_{ax} = l_{ba}\ddot{\varphi}_b - l_b\dot{\varphi}_b^2$, and $a_{az} = \ddot{z}_b + l_b\ddot{\varphi}_b + l_{ba}\dot{\varphi}_b^2$.

The acceleration at the mass center of link AB in horizontal and vertical directions can be given by

$$\begin{cases} a_{1x} = a_{ax} + l_{am}\varphi_1\sin\varphi_1 + l_{am}\dot{\varphi}_1^2\cos\varphi_1, \\ a_{1z} = a_{az} - l_{am}\varphi_1\cos\varphi_1 + l_{am}\dot{\varphi}_1^2\sin\varphi_1. \end{cases} \tag{24}$$

A set of state variables selected for analysis are listed below:

$$\begin{aligned}
u_1 &= z_a,\\
u_2 &= \varphi_a,\\
u_3 &= x_b,\\
u_4 &= z_b,\\
u_5 &= \varphi_b,\\
u_6 &= z_c,\\
u_7 &= \varphi_c,\\
u_8 &= z_d,\\
u_9 &= z_e,
\end{aligned} \tag{25a}$$

$$\begin{aligned}
u_{10} &= \dot{z}_a,\\
u_{11} &= \dot{\varphi}_a,\\
u_{12} &= \dot{x}_b,\\
u_{13} &= \dot{z}_b,\\
u_{14} &= \dot{\varphi}_b,\\
u_{15} &= \dot{z}_c,\\
u_{16} &= \dot{\varphi}_c,\\
u_{17} &= \dot{z}_d,\\
u_{18} &= \dot{z}_e.
\end{aligned} \tag{25b}$$

By substituting equations (25a) and (25b) into equations (2a)–(2d) and equations (19a)–(19c), the second-order differential equations can be reduced to the first order, which makes it easy to be handled mathematically.

4. Derivation Procedure of Model Parameters

In order to acquire the vertical stiffness and damping of tire, we simplify the tire to be a single-DOF dynamical system. By using the logarithmic decrement method of free vibration, the vertical stiffness and damping of front and rear tires can be gained. The site map and the test rig are demonstrated in Figure 6. The test rig system includes support frame (1), acceleration sensor (2), weight plate (3), rings (4), tire (5), rope (6), beam (7), linear bearing beam (8), displacement sensor (9), holder of sensor (10), suction plate (11), suspension bracket of magnetic lifter (12), magnetic lifter (13), ground (14), tire connection plate (15), linear bearing (16), and guide rods (17).

As can be seen in Figure 6, the under-test tire is supported by the beam. The weight plates are installed in the same way to inflict the load on the tire. The guide rod connects with the beam pass through the linear bearing. One end of the rope passes through the rings fixed to the lower side of the upper frame to suspend the under-test tire, and the other end is fastened to the suction plate. The cup of the suction plate is absorbed on the lower surface of the magnetic elevator that is mounted to the suspension bracket. For the purpose of eliminating the influence of gravity on the under-test tire, the magnetic lift is adjusted by operators depending on the situation. By regulating the height of the linear bearing beam, tires with different diameters can be installed by the test bed. The acceleration signal of the tire is acquired and saved by the data acquisition card. The test software is programmed with Labview code [44].

When the tire is lifted above the ground with a height h, the lower beam with the guide rod will fall along the guide sleeve due to gravity. After the tire hits the ground block, the vibration in time domain begins to attenuate freely and is collected using an acceleration sensor fixed to the beam. The log reduction can be calculated as

$$\delta = \frac{\ln\left(A_i/A_j\right)}{j-i} = \frac{\ln\left(\ddot{z}_i/\ddot{z}_j\right)}{j-i}. \tag{26}$$

The damping ratio of the system can be obtained based on the logarithmic decrement and is given by

$$\xi = \frac{\delta}{\sqrt{\delta^2 + (2\pi)^2}}. \tag{27}$$

Then, the vertical stiffness and damping of front and rear tires can be given by

$$\begin{aligned}
k &= \frac{(2\pi/T)^2\,\mathrm{m}}{1-\xi^2},\\
c &= 2\xi\sqrt{\mathrm{km}}.
\end{aligned} \tag{28}$$

With the first lag introduced, the dynamic response of the tested tire in the longitudinal direction can be given by

$$\frac{\sigma_\gamma \dot{F}_x}{v} + F_x = C_\gamma \gamma, \tag{29}$$

where γ is the slip of tire in the longitudinal direction, $\gamma = (r\dot{\theta} - \dot{x})/v$, r is the tire radius, $\dot{x}$ is the longitudinal tire speed, $\dot{\theta}$ represents the tire's roll speed, and v is the forward speed of tractor.

The longitudinal stiffness and damping of tire can be expressed as

$$\begin{aligned}
k_x &= \frac{C_\gamma}{\sigma_\gamma},\\
c_x &= \frac{C_\gamma}{v}.
\end{aligned} \tag{30}$$

Similarly, the site map of stiffness and damping test rig for rubber rings between the cabin and the chassis is shown in Figure 7, and the vertical stiffness and damping of the driver seat can also be obtained in the same way (Figure 8).

The stiffness and damping of silent blocks of the cabin and driver seat can be given by

$$\begin{aligned}
k_c &= \frac{m\omega^2\left(\alpha^2 - \alpha\cos\varphi\right)}{\alpha^2 - 2\alpha\cos\varphi + 1},\\
c_c &= \frac{m\omega\alpha\sin\varphi}{\alpha^2 - 2\alpha\cos\varphi + 1},
\end{aligned} \tag{31}$$

where α is the acceleration amplitude ratio between output and input signals, ω is the excitation frequency, m is the mass

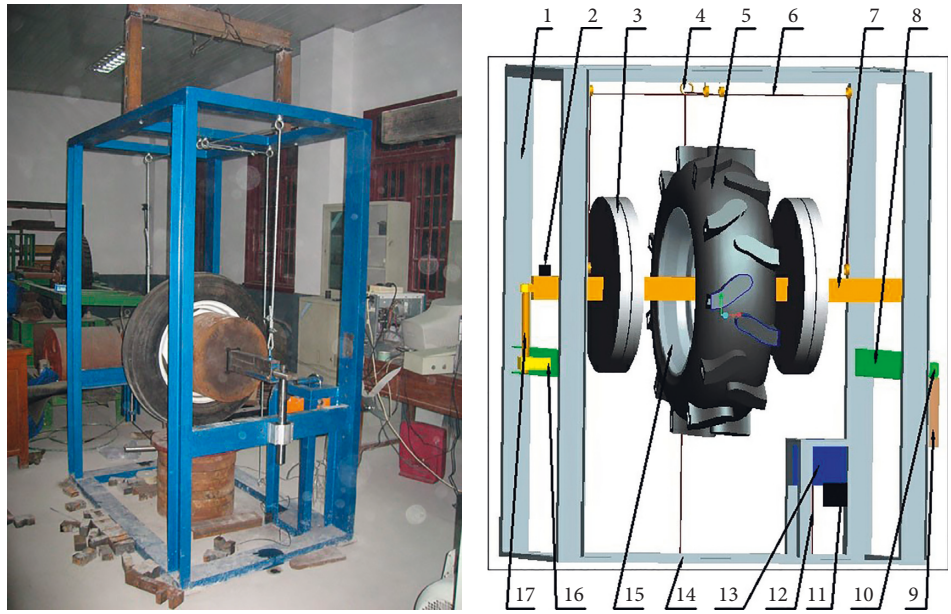

(a) (b)

Figure 6: Test device of stiffness and damping for tire: (a) site map; (b) structure principle.

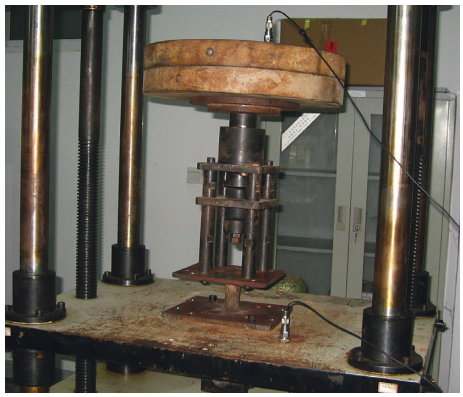

Figure 7: Site map of stiffness and damping test rig for the rubber suspension.

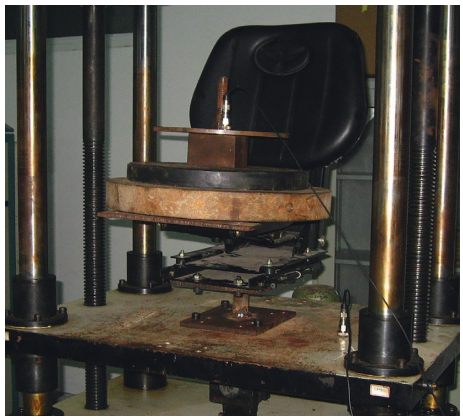

Figure 8: Site map of stiffness and damping test rig for the driver seat.

of the driver seat, and φ is the phase difference of output acceleration with respect to input acceleration.

The mean value of the measured modal parameters between 4 and 8 Hz, which is very sensitive to the health of the driver, can be used as the stiffness and damping parameters of simulation.

In order to obtain the mass and moment of inertia of wheeled tractor, its three-dimensional physical model is established in Pro/E software [45]. When the material property of each part for wheeled tractor is defined, the parameter of mass and the moment of inertia can be calculated easily.

5. Results and Discussion

The CF700 wheeled tractor system equipped with the implement and front axle hydropneumatic suspension as well as passive rubber cabin suspension is modeled in the numerical example. The corresponding parameters are listed in Table 1. A standard artificial test track with a length of 100 m, as shown in Figure 9, is employed to produce road excitations, which are applied to both front and rear tires of the tractor system.

When the forward speed of the tractor/implement system is 2 m/s and the nitrogen pressure and volume of the accumulators A and B are 6 MPa and 0.5 L, the measured and predicted acceleration values of the driver seat, cabin, chassis, and implement and their corresponding power spectral density (PSD) with the orifice diameter 2.4 mm of throttle valves 6 and 8 and 0 mm of throttle valve 9 (closed) for front axle hydropneumatic suspension are shown in Figures 10 and 11.

As can be seen from Figures 10 and 11, there are slight quantitative variations between the simulation time series

Table 1: Parameters of the wheeled tractor/implement with front axle hydropneumatic suspension.

l_f	1348 mm
l_r	840 mm
l_{bf}	360 mm
l_{br}	840 mm
k_f	357177 N/m
c_r	2516.8 N·s/m
k_{cr}	1012383 N/m
c_d	1473 N·s/m
I_a	166.67 kg·m^2
l_{bc}	0.14 m
l_1	0.42 m
l_{cd}	0.604 m
l_5	0.343 m
l_{cm}	0.302 m
C_d	0.7
A_9	0 m^2
P_{B0}	6 MPa
F_s	220 N
l_f	1348 mm
l_r	840 mm
l_{cf}	600 mm
l_{cr}	290 mm
l_d	290 mm
m_b	2694 kg
c_f	1789.2 N·s/m
k_{cf}	1012383 N/m
c_{cr}	5093 N·s/m
m_a	300 kg
γ	1.4775 rad
l_{ag}	0.576 m
l_2	0.42 m
l_3	0.125 m
l_6	0.287 m
D	0.05 m
ρ	900 kg/m^3
P_{A0}	6 MPa
V_{B0}	0.5 L
f_v	2
l_{cf}	600 mm
l_{cr}	290 mm
m_c	375 kg
m_d	75 kg
I_b	3249.3 kg·m^2
I_c	218.8 kg·m^2
k_r	359304 N/m
c_{cf}	5093 N·s/m
$A_7 + A_8$	4.52×10^{-6} m^2
m_e	146 kg
l_{ba}	0.21 m
l_b	0.94 m
l_{ab}	0.84 m
l_4	0.338 m
l_{am}	0.42 m
d	0.032 m
$A_5 + A_6$	4.52×10^{-6} m^2
V_{A0}	0.5 L
F_c	100 N
$\dot{x}_s$	0.003 m/s
m_c	375 kg
m_d	75 kg

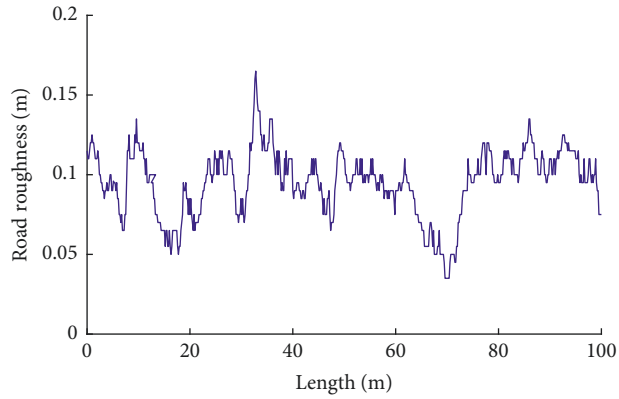

Figure 9: Road roughness of the standard artificial test track.

and the measured values generally. The vibration responses from the proposed model are in good agreement with experimental results, and the validity of the presented model in this work is verified. A pronounced resonant frequency was observed around 2–4 Hz for the tractor/implement system. To prove the proposed model further, the experimental and the predicted root mean square (RMS) values of acceleration for the tractor under different forward speeds are compared (Figure 12). It is demonstrated that the presented model is also effective in predicting the vibration characteristics of the tractor under different forward speeds. With the increase of the forward speed, the RMS values of acceleration for the driver seat, cabin, chassis, and implement increase dramatically and the RMS of cabin's acceleration is less than that of acceleration for the driver seat, chassis, and implement due to the passive rubber suspension between the cabin and chassis.

To evaluate the driver comfort of the tractor system, the frequency-weighted acceleration in the time domain is used to describe the exposure of the seated driver to the vertical vibration. Two typical weightings are often applied in practice: W_k is defined in the International Standard ISO 2631 [7] and W_b from British Standard, BS 6841 [8]. The RMS vibration magnitudes were determined for the vertical vibration simulated on the cabin floor and surface of the seat based on International Standard ISO 2631:

$$\mathrm{RMS} = \left[\frac{\int_0^T a^2(t)dt}{T}\right]^{1/2}, \tag{32}$$

where $a(t)$ is the frequency-weighted acceleration in time domain and T is the measurement period.

The SEAT values were calculated as the ratio of the frequency-weighted acceleration on the seat, $\mathrm{RMS}_{\mathrm{seat}}$, to the frequency-weight acceleration on the tractor floor, $\mathrm{RMS}_{\mathrm{floor}}$:

$$\mathrm{SEAT}_{\mathrm{RMS}}\% = \frac{\mathrm{RMS}_{\mathrm{seat}}}{\mathrm{RMS}_{\mathrm{floor}}}\%. \tag{33}$$

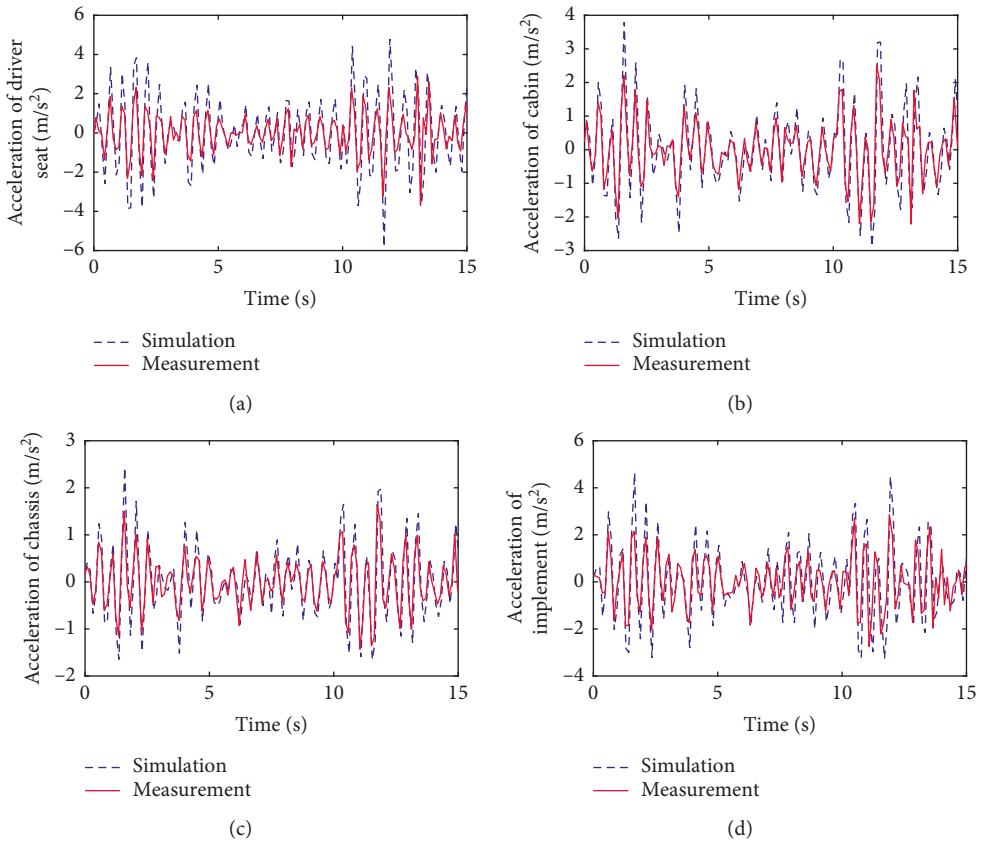

Figure 10: Vibration acceleration of the tractor/implement system: (a) driver seat; (b) cabin; (c) chassis; (d) implement.

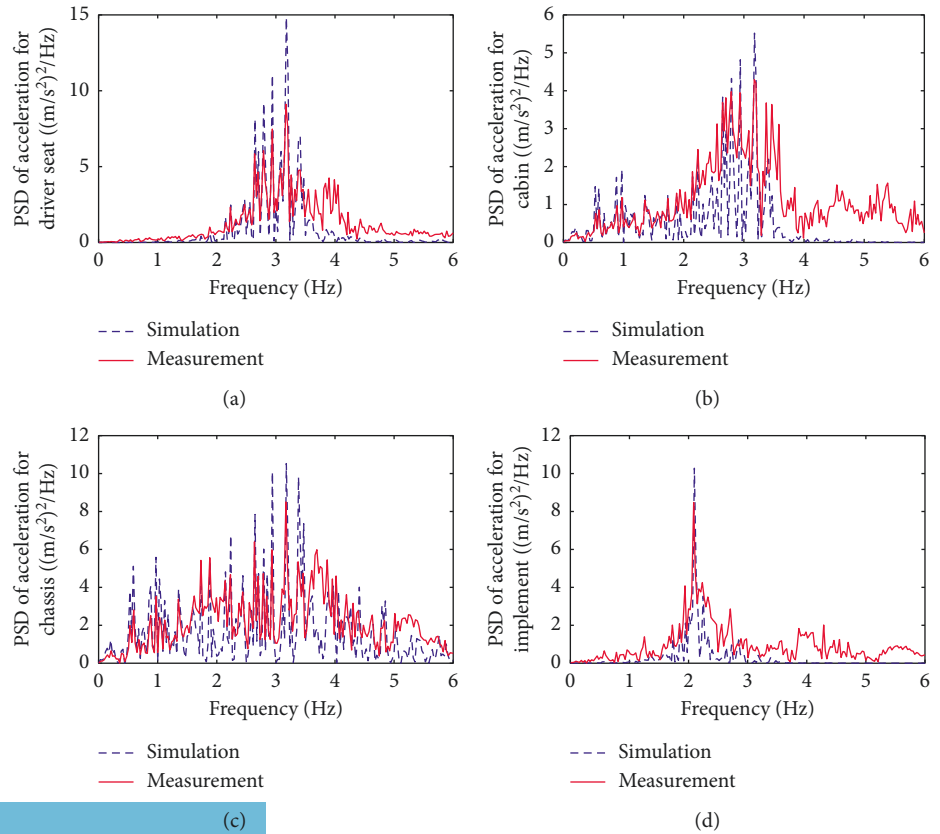

Figure 11: PSD of acceleration for the tractor/implement system: (a) driver seat; (b) cabin; (c) chassis; (d) implement.

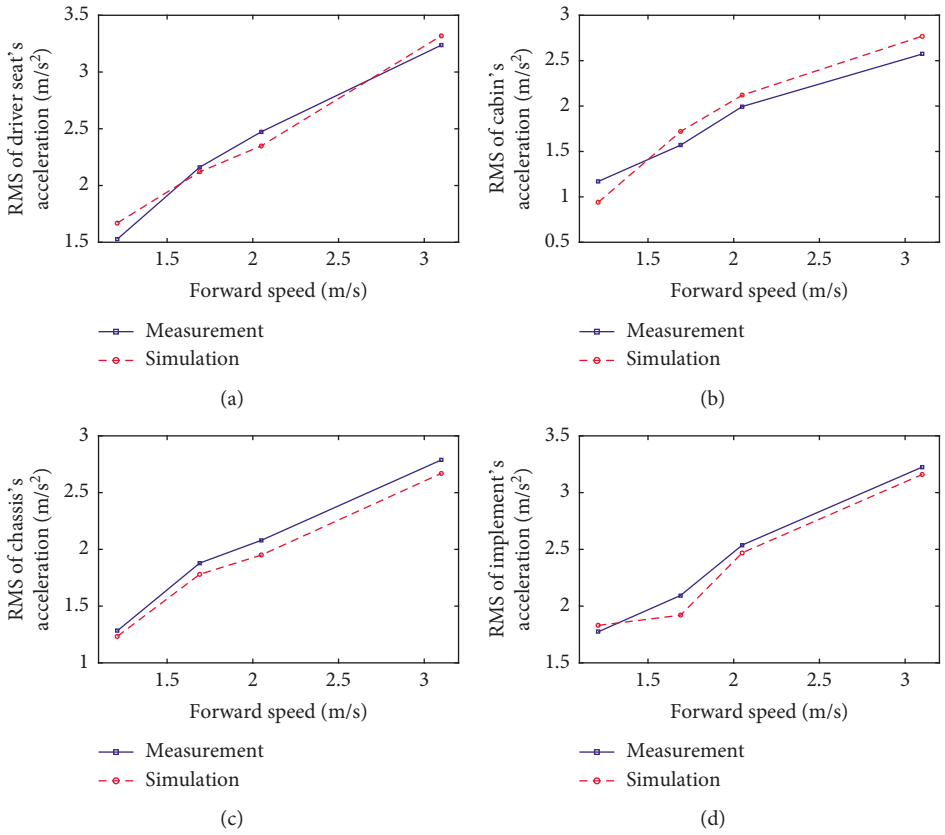

FIGURE 12: RMS of vibration responses for the tractor system under different forward speeds: (a) driver seat; (b) cabin; (c) chassis; (d) implement.

The SEAT value is used to describe the effectiveness of the driver seat, and the SEAT value below 100% implies that the seat is isolating vibration on the floor and thus reducing discomfort from the tractor vibration.

To make a comparative study on the effect of the passive cabin suspension, implement, and front axle hydropneumatic suspension on the vibration characteristics and driver comfort of the tractor system, the dynamic models of tractor system under such four cases as (I) without cabin, front axle suspension, and implement, (II) with cabin suspension and without front axle suspension and implement, (III) with cabin suspension and implement and without front axle suspension, and (IV) with cabin, front axle suspension, and implement are developed. The corresponding RMS values of vibration responses and SEAT values for the tractor/implement system under different settings are listed in Table 2.

Table 2 shows that the front axle hydropneumatic suspension increases the RMS of vertical vibration acceleration for the driver seat under the case with cabin and front axle suspension as well as implement compared with the case without front axle hydropneumatic suspension; meanwhile, the front axle hydropneumatic suspension decreases the RMS of longitudinal, vertical, and pitch vibrations for the chassis as well as dynamic load for front and rear tires dramatically. The passive cabin suspension can reduce the RMS of vertical vibration of the driver seat and longitudinal and vertical vibrations of the chassis, while increasing the RMS of pitch vibration for the chassis, dynamic loads for front and rear tires, and SEAT value tremendously compared with the case without cabin, front axle suspension, and implement. The RMS values of the vertical vibration for the driver seat, longitudinal, vertical, and pitch vibrations for the chassis, and SEAT value under the case II is larger than those under the case III, but the RMS values of dynamic loads for front and rear tires are on the contrary. Therefore, the front axle hydropneumatic suspension will deteriorate the ride comfort of the driver but will improve the handing stability obviously. The passive cabin suspension plays a more important role in improving the ride comfort of the driver than the front axle hydropneumatic suspension does, while taking the expense of operational stability to some extent. The existence of the implement will raise the comfortableness of the driver and worsen the corresponding handing stability at the same time dramatically. The calculated SEAT values indicated that the driver seat increases the vibration transmitted to the driver.

5.1. Effect of Nitrogen Volume of Accumulators. When the forward speed of the tractor system is 1.21 m/s and the nitrogen pressure of accumulators A and B is 6 MPa,

Table 2: RMS of vibration responses and SEAT values for the tractor/implement system under different settings.

Settings	$\ddot{z}_d$ (m/s^2)	$\ddot{x}_b$ (m/s^2)	$\ddot{z}_b$ (m/s^2)	$\ddot{\varphi}_b$ (rad/s^2)	F_{fdyn} (N)	F_{rdyn} (N)	SEAT
Case I	2.3942	2.0311	2.1048	0.9355	4335.2	2669.3	1.184
Case II	2.1700	1.5341	1.6914	1.1003	5342.8	4082.6	1.416
Case III	1.5697	1.40231	1.3742	0.8580	12080	7201.8	1.293
Case IV	2.6330	1.2562	1.5372	0.5240	4342.5	3484.5	1.851

the RMS values of vibration responses and SEAT values for the tractor/implement system with the orifice diameter 2.4 mm of throttle valves 6 and 8 and 0 or 5 mm of throttle valve 9 (closed or fully opened) for front axle hydropneumatic suspension under different initial nitrogen volumes of accumulators A and B are shown in Figure 13.

Figure 13 shows that when the throttle valve 9 is closed, the RMS values of vertical vibration for the driver seat, longitudinal, vertical, and pitch vibration for the chassis, dynamic load for front and rear tires, dynamic deflection for suspension, and SEAT values of the driver seat almost remain constant with the increase in nitrogen volume of the accumulators A and B. When the throttle valve 9 is fully opened, the RMS values of vertical vibration for driver seat and chassis, pitch vibration for the chassis, and SEAT values of the driver seat decrease dramatically with the increase in nitrogen volume of the accumulators A and B, while RMS values of dynamic loads for front and rear tires and dynamic deflection for suspension also remain constant. The RMS of longitudinal acceleration for the chassis increases and then decreases with the increase in nitrogen volume of the accumulators A and B. Therefore, the RMS values of vertical vibration for the driver seat, longitudinal, vertical, and pitch vibrations for the chassis, and SEAT values of the driver seat with the throttle valve fully opened are more sensitive to the change of initial nitrogen volume of the accumulators A and B than those with the throttle valve closed, while other RMS values of vibration responses for the tractor system are insensitive to the change of initial nitrogen volume of accumulators and almost remain constant regardless of the throttle valve being closed or opened. The optimized initial nitrogen volume for the front axle hydropneumatic suspension is 0.7 L when the throttle valve 9 is fully opened.

5.2. Effect of Nitrogen Pressure of Accumulators. When the forward speed of the tractor system is 1.21 m/s and the initial nitrogen volumes of the accumulators A and B is 0.5 L, the RMS values of vibration responses and SEAT values for the tractor/implement system with a 2.4 mm orifice diameter of throttle valves 6 and 8 for front axle hydropneumatic suspension under different nitrogen pressures of the accumulators A and B are shown in Figure 14.

It can be seen that when the throttle valve 9 is fully opened, the RMS values of vertical vibration for the driver seat and longitudinal, vertical, and pitch vibrations for the chassis decrease first and then increase with the initial nitrogen pressure ranging from 5.8 MPa to 6.2 MPa and continue to decrease with the increase of initial nitrogen pressure in the interval above 6.2 MPa, while RMS values of dynamic loads for front and rear tires, dynamic deflection for suspension, and SEAT values of the driver seat decrease. When the throttle valve 9 is closed, RMS of vibration responses (except longitudinal acceleration of the chassis) for the tractor system also remains constant with the increase of initial nitrogen pressure for the accumulators A and B. Therefore, only the RMS values of vertical vibration for the driver seat, longitudinal, vertical, and pitch vibrations of the chassis, and SEAT value of the driver seat when the throttle valve is fully opened are sensitive to the change of initial nitrogen pressure of the accumulators A and B. The optimized initial nitrogen pressure for the front axle hydropneumatic suspension when the throttle valve 9 is fully opened is 6.5 MPa.

5.3. Effect of Orifice Diameter of Throttle Valves 6 and 8. In this section, the effect of orifice diameter of throttle valves 6 and 8 is studied. When the forward speed of the tractor system is 1.21 m/s and the nitrogen pressure of the accumulators A and B is 6 MPa, the RMS values of vibration responses and SEAT values of the tractor/implement system with a 0.5 L initial nitrogen volume of the accumulators A and B under different orifice diameters of the throttle valves 6 and 8 are shown in Figure 15.

Figure 15 shows that when the throttle valve 9 is closed, the RMS values of vertical vibration for the driver seat and chassis, dynamic loads for front and rear tires, and SEAT values of driver seat decrease with the orifice diameter of the throttle valves 6 and 8 changing between 1 mm and 2 mm and continue to increase with the increase of orifice diameter of throttle valves 6 and 8 in the interval above 2 mm, while the RMS of longitudinal and pitch vibrations for the chassis rises obviously with the increase of orifice diameter of throttle valves 6, 8. When the throttle valve 9 is fully opened, the RMS values of vibration responses (except the dynamic load of the rear tire and dynamic deflection of the suspension) and SEAT values for the tractor system increase with an increase in the orifice diameter of throttle valves 6 and 8. Therefore, the recommended orifice diameter of throttle valves 6 and 8 is 2 mm when the throttle is closed to obtain the optimized ride comfort. When the throttle valve 9 is fully opened, the smaller the orifice diameter of the throttle valves 6 and 8 is, the better the ride comfort would be.

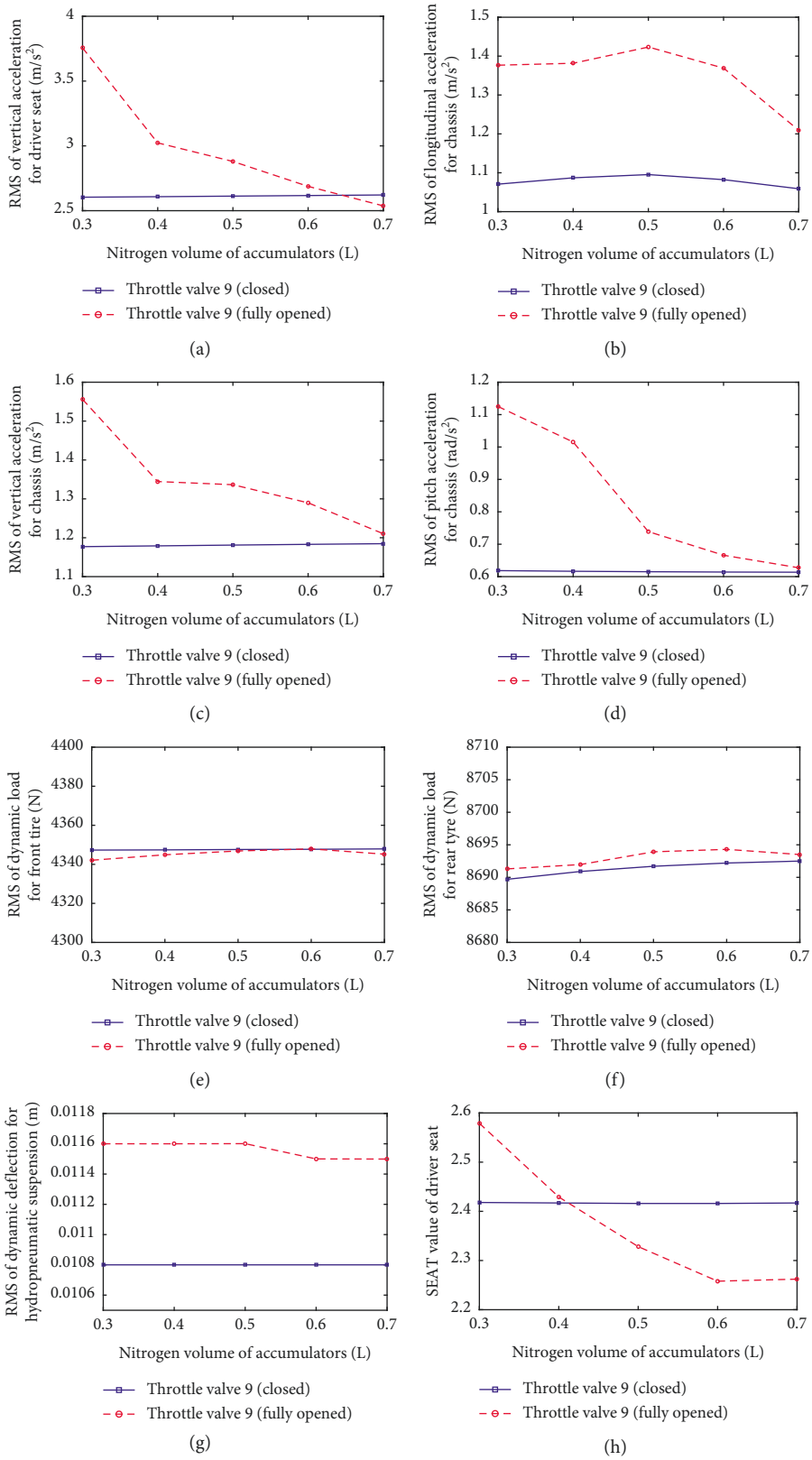

FIGURE 13: RMS of vibration responses of the tractor system under different initial nitrogen volumes of accumulators: (a) vertical acceleration of the driver seat; (b) longitudinal acceleration of the chassis; (c) vertical acceleration of the chassis; (d) pitch acceleration of the chassis; (e) dynamic load of the front tire; (f) dynamic load of the rear tire; (g) dynamic deflection of the hydropneumatic suspension; (h) SEAT value of the driver seat.

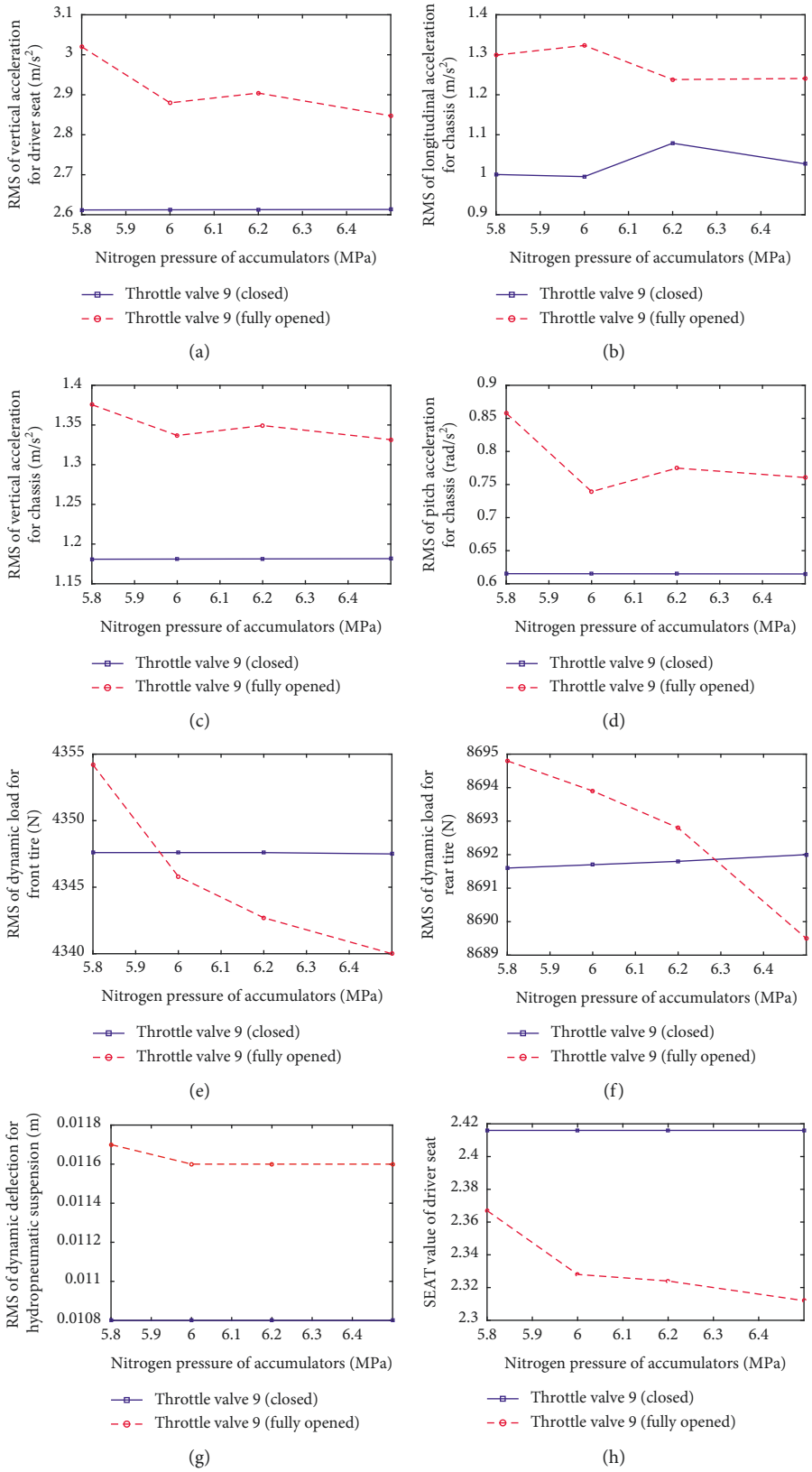

Figure 14: RMS of vibration responses of tractor system under different nitrogen pressure of the accumulators: (a) vertical acceleration of the driver seat; (b) longitudinal acceleration of the chassis; (c) vertical acceleration of the chassis; (d) pitch acceleration of the chassis; (e) dynamic load of the front tire; (f) dynamic load of the rear tire; (g) dynamic deflection of the hydropneumatic suspension; (h) SEAT value of the driver seat.

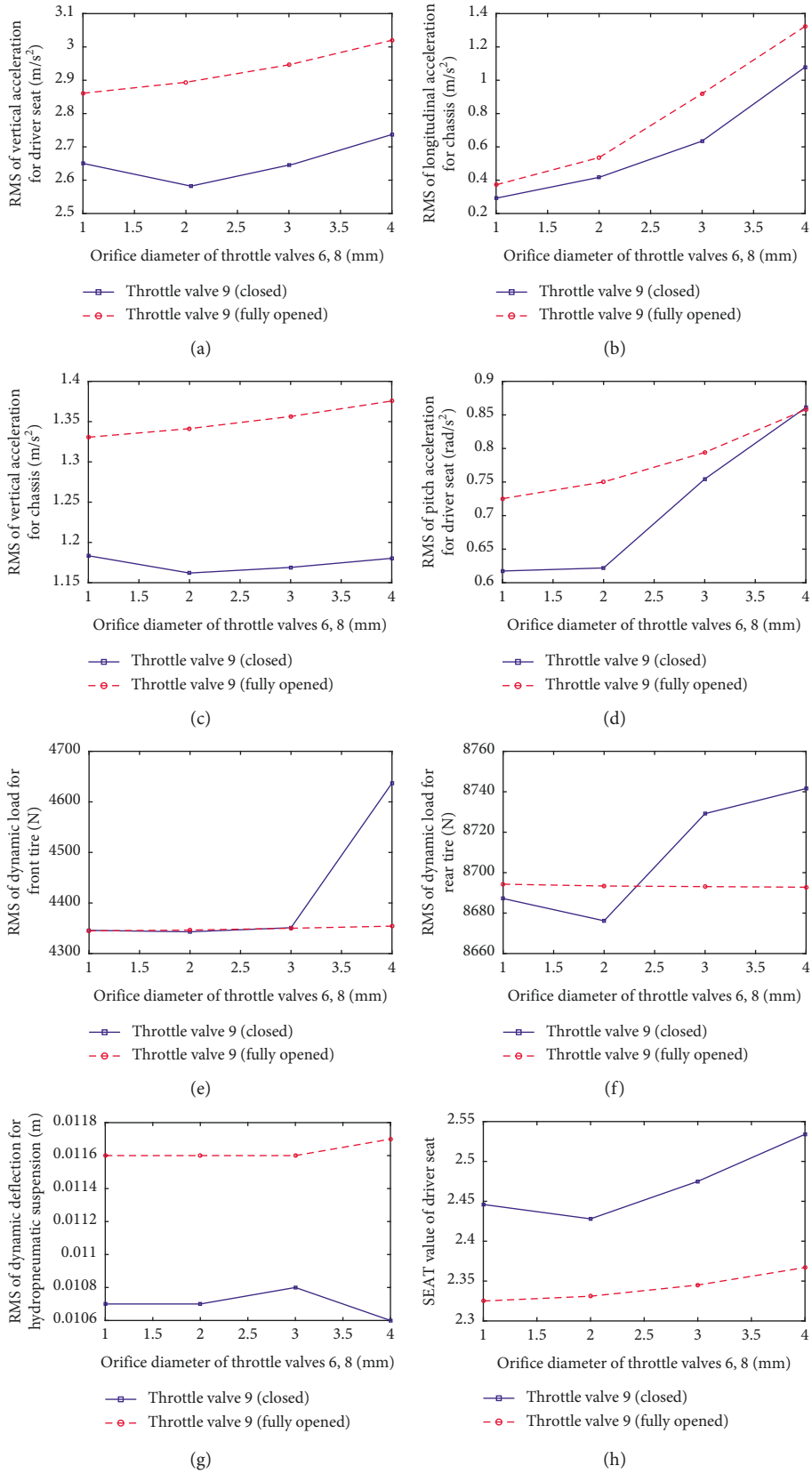

Figure 15: RMS of vibration responses of tractor system under different orifice diameters of throttle valves: (a) vertical acceleration of the driver seat; (b) longitudinal acceleration of the chassis; (c) vertical acceleration of the chassis; (d) pitch acceleration of the chassis; (e) dynamic load of the front tire; (f) dynamic load of the rear tire; (g) dynamic deflection of the hydropneumatic suspension; (h) SEAT value of the driver seat.

6. Conclusion

In this paper, a complete dynamic model of the wheeled tractor/implement system with front axle hydraulic-pneumatic suspension is established with the three-point suspension structure and the nonlinear effect of the front axle hydraulic suspension considered. Numerical and experimental results show that the model can be used to predict the vibration characteristics of real structures, and a pronounced resonant frequency was observed around 2–4 Hz for the tractor/implement system. The influences of the passive cabin suspension, the implement, and the hydraulic suspension of the front axle on the dynamic behaviour of the tractor system are studied and compared in four cases. The numerical example manifests that the front axle hydraulic suspension does not improve the driver's ride comfort but it significantly improves the steering stability. The passive cabin suspension contributes more to enhancing the ride comfort than the front axle oil and gas suspension do, while sacrificing operational stability to some extent. Because of the implement, the driver's comfort is improved, but the steering stability is lessened. The calculated SEAT values indicate that the driver seat increases the vibration transmitted to a driver. When the throttle valve 9 is fully opened, the initial nitrogen volume is 0.7 L and the optimized pressure of the front axle hydraulic suspension is 6.5 MPa. The dynamic load of front and rear tires and dynamic deflection of front axle hydraulic-pneumatic suspension are not sensitive to the change of the initial nitrogen volume and pressure of accumulators whether the throttle is closed or open. When the throttle is closed, the diameter of the recommended orifices of the throttles 6 and 8 should be 2 mm for the optimum ride comfort. When the throttle valve 9 is fully opened, the smaller the diameter of the holes of the throttle valves 6 and 8 is, the better the ride comfort will be.

Nomenclature

k_f, k_r: Stiffness of the front and rear tire
γ: Angular between linkages AB and EF
k_{cf}, k_{cr}: Stiffness of the front and rear cabin suspension
$\ddot{\varphi}_b$: Pitch vibration acceleration of the cabin
c_f, c_r: Damping of the front and rear tires
c_{cf}, c_{cr}: Damping of the front and rear cabin suspensions
l_{ba}, l_{bc}: Distance between mass center of the chassis plate and point A and between mass center of the chassis plate and point C in the vertical direction, respectively
l_{ag}, l_b: Distance between points A and G in the vertical direction and between mass center of the chassis plate and point A in the horizontal direction
m_a, m_b, m_c, m_d, m_e: Mass of the implement, chassis, cabin, driver, and front axle
l_1, l_2: Distance between points A and E and between points E and B, respectively
k_d, c_d: Stiffness and damping of the driver seat
l_{ab}, l_{cd}: Length of linkages AB and CD
I_a, I_b, I_c, I_d: Moment of inertia of the mass center of the implement, chassis, cabin, and driver
l_3, l_4: Distance between mass center of the implement and point B in the horizontal and vertical directions
φ_a, φ_b, φ_c: Pitch angle around mass center of the implement, chassis, and cabin
l_5, l_6: Distance between mass center of the implement and point D in the vertical and horizontal directions
z_a, z_b, z_c, z_d, z_e: Vertical displacement of mass center of the implement, chassis, cabin, driver, and front axle
l_{am}, l_{cm}: Distance between point A and mass center of linkage AB and between point C and mass center of linkage CD
l_{cf}, l_{cr}: Distance between the front cabin suspension and mass center of the cabin and between the rear cabin suspension and mass center of cabin
φ_1, φ_2: Rotational angle between horizontal direction and line AB and between horizontal direction and line CD
F_{fdyn}, F_{rdyn}: Dynamic load of the front and rear tires
l_f, l_r: Distance between the front axle and mass center of the chassis and between rear axle and mass center of the chassis
$\ddot{z}_a$, $\ddot{z}_b$, $\ddot{z}_c$, $\ddot{z}_d$, $\ddot{z}_e$: Vertical vibration acceleration of the implement, chassis, cabin, driver, and front axle
f_{fas}: Dynamic deflection of front axle hydropneumatic suspension
x_b: Longitudinal displacement of mass center of the cabin.

Data Availability

The data used to support the findings of this study are available from the corresponding author upon request.

Conflicts of Interest

The authors declare that they have no conflicts of interest.

Acknowledgments

This paper has been partially supported by the following projects: "China Postdoctoral Fund," grant no. 2016M591855, "Jiangsu Province Postdoctoral Research Funding Schemes," grant no. 1401049B, and "National Natural Science Foundation of China," grant no. 51275249.

References

[1] N. Prasad, V. K. Tewari, and R. Yadav, "Tractor ride vibration-a review," *Journal of Terramechanics*, vol. 32, no. 4, pp. 205–219, 1995.

[2] M. Muzammil, S. S. Siddiqui, and F. Hasan, "Physiological effect of vibrations on tractor drivers under variable ploughing conditions," *Journal of Occupational Health*, vol. 46, no. 5, pp. 403–409, 2004.

[3] A. J. Scarlett, J. S. Price, and R. M. Stayner, "Whole-body vibration: evaluation of emission and exposure levels arising from agricultural tractors," *Journal of Terramechanics*, vol. 44, no. 1, pp. 65–73, 2007.

[4] D. M. Cuong, S. Zhu, and N. T. Ngoc, "Study on the variation characteristics of vertical equivalent damping ratio of tire-soil system using semi-empirical model," *Journal of Terramechanics*, vol. 51, pp. 67–80, 2014.

[5] P. Farhadi, A. Golmohammadi, A. Sharifi, and G. Shahgholi, "Potential of three-dimensional footprint mold in investigating the effect of tractor tire contact volume changes on rolling resistance," *Journal of Terramechanics*, vol. 78, pp. 63–72, 2018.

[6] H. Taghavifar and A. Mardani, "Investigating the effect of velocity, inflation pressure, and vertical load on rolling resistance of a radial ply tire," *Journal of Terramechanics*, vol. 50, no. 2, pp. 99–106, 2013.

[7] ISO 2631-1, *Mechanical Vibration and Shock-Evaluation of Human Exposure to Whole-Body Vibration*, International Organization for Standardisation, Geneva, Switzerland, 1997.

[8] BS 6841, *Measurement and Evaluation of Human Exposure to Whole-Body Mechanical Vibration and Repeated Shock*, British Standards Institution, London, UK, 1987.

[9] J. Lines, M. Stiles, and R. Whyte, "Whole body vibration during tractor driving," *Journal of Low Frequency Noise, Vibration and Active Control*, vol. 14, no. 2, pp. 87–104, 1995.

[10] J. Arvidsson and S. Ristic, "Soil stress and compaction effects for four tractor tyres," *Journal of Terramechanics*, vol. 33, no. 5, pp. 223–232, 1996.

[11] A. Kumar, P. Mahajan, D. Mohan, and M. Varghese, "IT-information technology and the human interface," *Journal of Agricultural Engineering Research*, vol. 80, no. 4, pp. 313–328, 2001.

[12] A. Marsili, L. Ragni, G. Santoro, P. Servadio, and G. Vassalini, "PM-power and machinery," *Biosystems Engineering*, vol. 81, no. 1, pp. 35–47, 2002.

[13] R. Hildebrand, E. Keskinen, and J. A. R. Navarrete, "Vehicle vibrating on a soft compacting soil half-space: ground vibrations, terrain damage, and vehicle vibrations," *Journal of Terramechanics*, vol. 45, no. 4, pp. 121–136, 2008.

[14] L. L. Clijmans, H. H. Ramon, and J. J. De Baerdemaeker, "Structural modification effects on the dynamic behavior of an agricultural tractor," *Transactions of the ASAE*, vol. 41, no. 1, pp. 5–10, 1998.

[15] M. Cutini, C. Costa, and C. Bisaglia, "Development of a simplified method for evaluating agricultural tractor's operator whole body vibration," *Journal of Terramechanics*, vol. 63, pp. 23–32, 2016.

[16] S. A. Adam and N. A. A. Jalil, "Vertical suspension seat transmissibility and seat values for seated person exposed to whole-body vibration in agricultural tractor preliminary study," *Procedia Engineering*, vol. 170, pp. 435–442, 2017.

[17] D. M. Cuong, S. Zhu, and Y. Zhu, "Effects of tyre inflation pressure and forward speed on vibration of an unsuspended tractor," *Journal of Terramechanics*, vol. 50, no. 3, pp. 185–198, 2013.

[18] M. Zehsaz, M. H. Sadeghi, M. M. Ettefagh, and F. Shams, "Tractor cabin's passive suspension parameters optimization via experimental and numerical methods," *Journal of Terramechanics*, vol. 48, no. 6, pp. 439–450, 2011.

[19] C. Spelta, F. Previdi, S. M. Savaresi et al., "Performance analysis of semi-active suspensions with control of variable damping and stiffness," *Vehicle System Dynamics*, vol. 49, no. 1-2, pp. 237–256, 2011.

[20] V. N. Nguyen and S. Inaba, "Effects of tire inflation pressure and tractor velocity on dynamic wheel load and rear axle vibrations," *Journal of Terramechanics*, vol. 48, no. 1, pp. 3–16, 2011.

[21] Y. Yang, W. Ren, L. Chen, M. Jiang, and Y. Yang, "Study on ride comfort of tractor with tandem suspension based on multi-body system dynamics," *Applied Mathematical Modelling*, vol. 33, no. 1, pp. 11–33, 2009.

[22] T. J. Lehtonen and M. Juhala, "Predicting the ride behaviour of a suspended agricultural tractor," *International Journal of Vehicle Systems Modelling and Testing*, vol. 1, no. 1–3, pp. 131–142, 2005.

[23] G. Shahgoli, J. Fielke, C. Saunders, and J. Desbiolles, "Simulation of the dynamic behaviour of a tractor-oscillating subsoiler system," *Biosystems Engineering*, vol. 106, no. 2, pp. 147–155, 2010.

[24] J. K. Hammond and R. F. Harrison, "Nonstationary response of vehicles on rough ground-a state space approach," *Journal of Dynamic Systems, Measurement, and Control*, vol. 103, no. 3, pp. 245–250, 1981.

[25] J. Q. Yuan, S. H. Zhu, Q. Gao, G. Xu, J. F. Ma, and Z. X. Lu, "Design and characteristic study of tractor front axle hydropneumatic spring," *Journal of Nanjing Agricultural University*, vol. 40, no. 1, pp. 176–185, 2017.

[26] S. H. Zhu, S. Zwiebel, and G. Bernhardt, "A theoretical formula for calculating damping in the impact of two bodies in a multibody system," *Proceedings of the Institution of Mechanical Engineers, Part C: Journal of Mechanical Engineering Science*, vol. 213, no. 3, pp. 211–216, 1999.

[27] A. Rehnberg, *Suspension Design for Off-Road Construction Machines*, KTH Royal Institute of Technology, Stockholm, Sweden, 2011.

[28] M. Gobbi, G. Mastinu, and G. Previati, "Farm tractors with suspended front axle: anti-dive and anti-lift characteristics," *Journal of Terramechanics*, vol. 56, pp. 157–172, 2014.

[29] S. H. Zhu, G. Xu, J. Q. Yuan, J. F. Ma, and Y. Yilidaer, "Influence of implement's mass on vibration characteristics of tractor-implement system," *Transactions of the Chinese Society of Agricultural Engineering*, vol. 30, no. 24, pp. 30–37, 2014.

[30] E. Zheng, Y. Fan, R. Zhu, Y. Zhu, and J. Xian, "Prediction of the vibration characteristics for wheeled tractor with suspended driver seat including air spring and MR damper," *Journal of Mechanical Science and Technology*, vol. 30, no. 9, pp. 4143–4156, 2016.

[31] M. A. Rabbani, T. Tsujimoto, M. Mitsuoka, E. Inoue, and T. Okayasu, "Prediction of the vibration characteristics of half-track tractor considering a three-dimensional dynamic model," *Biosystems Engineering*, vol. 110, no. 2, pp. 178–188, 2011.

[32] S. Melzi, S. Negrini, and E. Sabbioni, "Numerical analysis of the effect of tire characteristics, soil response and suspensions tuning on the comfort of an agricultural vehicle," *Journal of Terramechanics*, vol. 55, pp. 17–27, 2014.

[33] Z. Li, M. Mitsuoka, E. Inoue, T. Okayasu, and Y. Hirai, "Development of stability indicators for dynamic Phase I overturn of conventional farm tractors with front axle pivot," *Biosystems Engineering*, vol. 134, pp. 55–67, 2015.
[34] K. Sim, H. Lee, J. W. Yoon, C. Choi, and S.-H. Hwang, "Effectiveness evaluation of hydro-pneumatic and semi-active cab suspension for the improvement of ride comfort of agricultural tractors," *Journal of Terramechanics*, vol. 69, pp. 23–32, 2017.
[35] O. B. Ahmed and J. F. Goupillon, "Predicting the ride vibration of an agricultural tractor," *Journal of Terramechanics*, vol. 34, no. 1, pp. 1–11, 1997.
[36] J. De Temmerman, K. Deprez, J. Anthonis, and H. Ramon, "Conceptual cab suspension system for a self-propelled agricultural machine, part 1: development of a linear mathematical model," *Biosystems Engineering*, vol. 89, no. 4, pp. 409–416, 2004.
[37] K. Deprez, D. Moshou, J. Anthonis, J. De Baerdemaeker, and H. Ramon, "Improvement of vibrational comfort on agricultural vehicles by passive and semi-active cabin suspensions," *Computers and Electronics in Agriculture*, vol. 49, no. 3, pp. 431–440, 2005.
[38] M. Martelli, R. Paoluzzi, and L. G. Zarotti, "The front suspension of agricultural tractors," in *Proceedings of the 14th International Conference of the International Society for Terrain-Vehicle Systems*, pp. 20–24, Vicksburg, MS, USA, October 2002.
[39] A. A. Mazhei, A. A. Uspenskiy, and V. G. Ermalenok, "Dynamic analysis of the hydro-pneumatic front axle suspension of agriculture tractor," in *Proceedings of the SAE Technical Paper Series*, pp. 1–6, Chicago, IL, USA, October 2006.
[40] N. J. Theron and P. S. Els, "Modelling of a semi-active hydropneumatic spring damper unit," *International Journal of Vehicle Design*, vol. 45, no. 4, pp. 501–521, 2007.
[41] S. F. van der Westhuizen and P. Schalk Els, "Comparison of different gas models to calculate the spring force of a hydropneumatic suspension," *Journal of Terramechanics*, vol. 57, pp. 41–59, 2015.
[42] Y. Yin, S. Rakheja, J. Yang, and P.-E. Boileau, "Characterization of a hydro-pneumatic suspension strut with gas-oil emulsion," *Mechanical Systems and Signal Processing*, vol. 106, pp. 319–333, 2018.
[43] Y. Yilidaer, S. H. Zhu, G. Xu, and J. Q. Yuan, "Front axle suspension parameters match and its impact on vibration characteristics of tractor," *Transactions of the Chinese Society of Agricultural Engineering*, vol. 31, no. 10, pp. 29–36, 2015.
[44] X. H. Chen and Y. H. Zhang, *LabVIEW 8.20 Programming from Getting Started to Proficient*, TsingHua University Press, Beijing, China, 2007.
[45] J. Sun, *Pro/Engineer 2000i Basic Design Tutorial*, TsingHua University Press, Beijing, China, 2001.